Research Square

Preprints are preliminary reports that have not undergone peer review.
They should not be considered conclusive, used to inform clinical practice,
or referenced by the media as validated information.

Integrated Plasma miR-15a-5p, Inflammatory Markers, and PBMC Cell-Cycle Genes for Distinguishing Active from Latent Tuberculosis: A Cross-Sectional Diagnostic Study

Xingcai Chen
Guilin people's Hospital
Lei Yang
Guilin people's Hospital
Jie Wang
Guilin Third People’s Hospital
Limin Zhai
Guilin people's Hospital
Jie Bai
Guilin people's Hospital
Jingwen Xiao
Guilin people's Hospital
Hao Zeng
Guigang City People's Hospital
Shanshan Liu
Guilin people's Hospital
Jun Yang
yangjun0930@gmail.com
Guilin people's Hospital

Research Article

Keywords: tuberculosis, latent tuberculosis infection, active tuberculosis, miR-15a-5p, CCND1, CCND2, peripheral blood mononuclear cells, diagnostic biomarkers

Posted Date: August 15th, 2026

DOI: https://doi.org/10.21203/rs.3.rs-10556327/v1

License: This work is licensed under a Creative Commons Attribution 4.0 International License.
Read Full License

Additional Declarations: No competing interests reported.

Abstract

Background

Distinguishing active tuberculosis (ATB) from latent tuberculosis infection (LTBI) remains challenging. This study evaluated plasma miR-15a-5p, inflammatory markers, and peripheral blood mononuclear cell (PBMC) cell-cycle-related genes as candidate biomarkers for tuberculosis classification.

Methods

In this single-centre cross-sectional diagnostic study, 50 patients with ATB, 50 individuals with LTBI, and 50 healthy controls were enrolled. Plasma and PBMC expression of miR-15a-5p, *CCND1*, *CCND2*, and *CDK6* was measured using RT-qPCR, while plasma C-reactive protein (CRP) and interleukin-6 (IL-6) were measured using routine clinical platforms. Diagnostic performance was assessed using receiver operating characteristic analysis. A multivariable logistic regression model combining plasma miR-15a-5p, CRP, and IL-6 was internally validated using 1,000 bootstrap resamples. Public miRNA and transcriptomic datasets were analysed to assess reproducibility, compartment specificity, and treatment-associated changes.

Results

Plasma miR-15a-5p, CRP, and IL-6 were significantly elevated in ATB. Plasma miR-15a-5p distinguished ATB from healthy controls with an area under the curve (AUC) of 0.846. In PBMCs, *CCND1* was downregulated and *CCND2* was upregulated in both LTBI and ATB, whereas *CDK6* showed no significant difference. For distinguishing ATB from LTBI, miR-15a-5p, CRP, and IL-6 individually yielded AUCs of 0.740, 0.756, and 0.793, respectively. Their combination achieved an AUC of 0.920, with a bootstrap-corrected AUC of 0.913, 90% sensitivity, 86% specificity, and 88% accuracy. Public datasets revealed compartment- and cell-subset-specific expression patterns, including a treatment-associated increase in classical-monocyte *CCND2*.

Conclusions

Plasma miR-15a-5p combined with CRP and IL-6 improved the discrimination of ATB from LTBI, while PBMC *CCND1* and *CCND2* reflected tuberculosis-associated transcriptional changes. External multicentre validation is required before clinical application.

1. Background

Tuberculosis (TB), a chronic infectious disease caused by *Mycobacterium tuberculosis* (MTB), remains a major public health threat worldwide[1, 2]. The clinical outcomes following MTB infection are highly

heterogeneous and may manifest as latent tuberculosis infection (LTBI) or active tuberculosis (ATB)[3]. Individuals with LTBI are generally asymptomatic and show no evidence of active disease; however, latent infection may reactivate and progress to ATB when host immune function becomes impaired[4]. Accurate identification of different tuberculosis infection states, particularly the distinction between LTBI and ATB, is therefore essential for early intervention, preventing disease transmission, and optimizing clinical management.

The diagnosis of tuberculosis currently relies primarily on microbiological, radiological, and immunological approaches[5]. Sputum smear microscopy, mycobacterial culture, and molecular assays can provide microbiological confirmation of ATB, but their sensitivity may be reduced in patients with low bacillary loads or inadequate sputum specimens[6]. The tuberculin skin test (TST) and interferon-gamma release assays (IGRAs) detect host immune responses to MTB antigens; however, they cannot reliably distinguish LTBI from ATB or adequately reflect disease activity[7]. Commonly used inflammatory markers, including C-reactive protein (CRP) and interleukin-6 (IL-6), may reflect systemic inflammation to some extent. Still, their limited specificity prevents their use as independent markers for classifying tuberculosis infection states[8]. Therefore, the identification of novel molecular biomarkers that reflect MTB infection status and facilitate the discrimination of LTBI from ATB remains an important focus of tuberculosis diagnostic research.

microRNAs (miRNAs) are endogenous non-coding RNA molecules approximately 18–25 nucleotides in length that regulate gene expression at the post-transcriptional level, primarily through binding to target mRNAs[9]. Their relative stability in plasma, serum, extracellular vesicles, and other biological fluids has led to growing interest in their potential as non-invasive biomarkers[10]. miR-15a-5p, a member of the miR-15/16 family, has been associated with cell-cycle regulation, apoptosis, inflammation, and immune responses[11–13]. In our previous study[14], high-throughput small RNA sequencing of plasma samples identified miR-15a-5p as one of the significantly upregulated miRNAs in patients with ATB. Target prediction and protein–protein interaction network analyses further identified the cell cycle–related genes *CCND1*, *CCND2*, and *CDK6* as candidate genes, with *CCND1* predicted as a potential target of miR-15a-5p.

Cell-cycle regulation is involved not only in cellular proliferation but also in immune-cell activation, differentiation, and functional remodeling [15]. CCND1 and CCND2 encode cyclin D1 and cyclin D2, respectively, which form complexes with cyclin-dependent kinases 4 and 6 to promote progression from the G1 phase to the S phase[16]. In addition to its classical role in cell-cycle regulation, CDK6 has been associated with immune cell differentiation, inflammatory responses, and host defense [17]. Studies conducted in various disease models have suggested that miR-15a-5p may directly or indirectly regulate cell-cycle-related genes, including CCND1, CCND2, and CDK6[18, 19]. Nevertheless, the diagnostic relevance of miR-15a-5p and its associated cell-cycle-related genes in tuberculosis infection, particularly their potential to distinguish LTBI from ATB, has not been systematically investigated.

In this context, the present study aimed to comprehensively characterize plasma miR-15a-5p expression and the expression of the cell-cycle-related genes CCND1, CCND2, and CDK6 in peripheral blood mononuclear cells (PBMCs), and to evaluate their expression patterns and diagnostic performance among healthy controls (HCs), individuals with LTBI, and patients with ATB. Their expression patterns and diagnostic performance were assessed, and a combined plasma model integrating miR-15a-5p, CRP, and IL-6 was developed to discriminate ATB from LTBI directly. Independent public miRNA and transcriptomic datasets were further analyzed to assess the reproducibility, cell-subset specificity, and treatment-associated changes of the candidate biomarkers.

2. Methods

2.1 Study Participants and Sample Collection

According to predefined inclusion and exclusion criteria, 50 patients with active tuberculosis (ATB) who presented for the first time and were clinically diagnosed at Guilin People's Hospital between January 2026 and May 2026 were consecutively enrolled in the ATB group. During the same period, 50 individuals with latent tuberculosis infection (LTBI) were enrolled in the LTBI group, and 50 healthy volunteers undergoing routine health examinations at the Health Management Center of Guilin People's Hospital were recruited as healthy controls (HCs). General clinical information, including age and sex, was collected for all participants. Baseline characteristics were compared among the three groups to assess comparability. The study was approved by the Medical Ethics Committee of Guilin People's Hospital (approval No. 2026002KY), and written informed consent was obtained from all participants.

Inclusion and Exclusion Criteria:

2.1.1. ATB Group

Patients with ATB were enrolled primarily according to the Chinese diagnostic standard for pulmonary tuberculosis (WS 288—2017), together with a comprehensive assessment of clinical symptoms, chest imaging findings, sputum smear microscopy, mycobacterial culture, molecular testing, and response to anti-tuberculosis treatment. The inclusion criteria were as follows: (1) age ≥ 18 years; (2) fulfilment of the clinical diagnostic criteria for active pulmonary tuberculosis, with tuberculosis-related clinical manifestations and/or radiological evidence of active pulmonary lesions; (3) evidence of *Mycobacterium tuberculosis* infection supported by sputum smear microscopy for acid-fast bacilli, mycobacterial culture, molecular testing, or other microbiological examinations, or a clinical diagnosis of active pulmonary tuberculosis based on comprehensive evaluation; (4) first presentation and no systematic anti-tuberculosis treatment before sample collection; and (5) voluntary participation and provision of written informed consent.

2.1.2. LTBI Group

LTBI was defined according to the World Health Organization principles for distinguishing tuberculosis infection from active tuberculosis disease, together with clinical assessment. The inclusion criteria were as follows: (1) age ≥ 18 years; (2) a positive interferon-gamma release assay (IGRA) and/or tuberculin skin test (TST); (3) absence of clinical symptoms suggestive of active tuberculosis, including cough, sputum production, haemoptysis, fever, night sweats, and weight loss; (4) no radiological evidence of active pulmonary tuberculosis; (5) no microbiological or clinical evidence supporting a diagnosis of active tuberculosis; and (6) voluntary participation and provision of written informed consent.

2.1.3. Exclusion Criteria for the ATB and LTBI Groups

Participants in the ATB and LTBI groups were excluded if they met any of the following criteria: (1) concomitant infectious diseases or major respiratory disorders, such as pneumonia, chronic obstructive pulmonary disease, or lung cancer; (2) previous anti-tuberculosis treatment; (3) recent vaccination, including bacillus Calmette–Guérin vaccination or other vaccinations potentially affecting immunological test results within the preceding 3 months; (4) human immunodeficiency virus infection or acquired immunodeficiency syndrome; (5) current treatment with glucocorticoids, immunosuppressants, biological agents, or other immunomodulatory therapies; (6) malignancy, autoimmune disease, severe hepatic or renal dysfunction, or other diseases that could affect immune status; (7) pregnancy or lactation; or (8) incomplete clinical or laboratory data.

2.1.4. HC Group

Healthy volunteers were recruited from individuals undergoing routine health examinations at the Health Management Center of Guilin People's Hospital during the same period. The inclusion criteria were as follows: (1) age ≥ 18 years; (2) generally good health, with no clinically significant abnormalities identified by physical examination or routine laboratory testing; (3) a negative IGRA result; (4) no history of tuberculosis, known tuberculosis exposure, or recent risk of tuberculosis infection; (5) no active infection, inflammatory disease, autoimmune disease, malignancy, or other condition potentially affecting immune status; (6) no current immunosuppressive treatment; and (7) voluntary participation and provision of written informed consent.

2.2 Plasma Sample Collection and Processing

A single 5-mL peripheral venous blood sample was collected from each participant under fasting conditions on the morning after enrolment and transferred into a vacuum tube containing dipotassium ethylenediaminetetraacetic acid (EDTA-K_2). After collection, the anticoagulated blood sample was gently mixed and divided into separate aliquots for plasma preparation and peripheral blood mononuclear cell (PBMC) isolation.

The aliquot intended for plasma preparation was centrifuged at 3,000 × *g* for 10 min. The upper plasma layer was carefully aspirated and transferred into RNase-free tubes without disturbing the buffy coat or introducing cellular components. Plasma samples were divided into aliquots of appropriate volumes to meet subsequent RNA extraction and testing requirements, minimizing repeated freeze–thaw cycles. All

aliquots were stored at − 80°C until RNA extraction and subsequent analysis. Samples showing visible hemolysis, coagulation, or insufficient volume were excluded from subsequent analyses.

2.3 PBMC Isolation and RNA Extraction

The remaining aliquot of the same EDTA-anticoagulated blood sample was used for PBMC isolation and was processed within 2 h of collection. The blood was gently mixed with an equal volume of sterile phosphate-buffered saline (PBS) and carefully layered over lymphocyte separation medium. PBMCs were isolated by density-gradient centrifugation. The mononuclear cell layer was carefully collected and washed twice with PBS to remove platelets and residual separation medium. After centrifugation, the PBMC pellet was either immediately subjected to RNA extraction or stored at − 80°C until further analysis.

Plasma RNA was extracted from an equal volume of plasma from each participant using the miRcute Serum/Plasma miRNA Isolation Kit (DP503; Tiangen Biotech Co., Ltd., Beijing, China) according to the manufacturer's instructions. RNase-free consumables were used throughout the procedure, and repeated freeze–thaw cycles were avoided.

Total RNA from PBMCs was extracted using TRIzol reagent (Invitrogen, USA). Briefly, PBMC pellets were completely lysed in an appropriate volume of TRIzol reagent, followed by chloroform extraction, isopropanol precipitation, and ethanol washing according to the manufacturer's instructions. The RNA pellet was dissolved in RNase-free water. RNA concentration and purity were assessed spectrophotometrically, and the A260/A280 ratio was recorded. RNA samples meeting the quality requirements were immediately used for reverse transcription or stored at − 80°C until use.

2.4 Reverse Transcription of miRNAs

Reverse transcription of miRNAs from plasma RNA and PBMC total RNA was performed using the Mir-X™ miRNA qRT-PCR TB Green® Kit (Takara Bio, Dalian, China) according to the manufacturer's instructions. This kit uses miRNA polyadenylation and a universal reverse-transcription system to convert mature miRNAs into complementary DNA (cDNA) for subsequent miRNA-specific quantitative PCR analysis.

Because plasma RNA concentrations were relatively low, an equal volume of RNA eluate from each plasma sample was used for reverse transcription to minimize bias resulting from differences in starting material. For PBMC RNA, the input volume was adjusted based on RNA concentration to ensure equal amounts of starting RNA across samples. All procedures were conducted under RNase-free conditions, and reaction mixtures were prepared on ice.

The miRNA reverse-transcription reaction mixture was prepared according to the manufacturer's protocol. After gentle mixing and brief centrifugation, the reaction was performed in a PCR thermal cycler. The resulting cDNA was either used immediately for quantitative PCR or stored at − 20°C until further analysis.

2.5 Reverse Transcription of mRNA

Reverse transcription of mRNA from plasma RNA and PBMC total RNA was performed using the All-in-One First-Strand Synthesis MasterMix with dsDNase (Cat. No. EG15133S; Yugong Biotech/BestEnzymes, China) according to the manufacturer's instructions. The system includes a dsDNase treatment step to remove residual genomic DNA, thereby minimizing its potential interference with subsequent qPCR analysis.

Because the concentration of cell-free RNA extracted from plasma was relatively low, an equal volume of plasma RNA eluate was used for each reverse-transcription reaction to minimize variation in starting material among samples. For PBMC RNA, each reaction contained 1 μg of total RNA, and the corresponding reaction volume was calculated based on the measured RNA concentration. Nuclease-free water was added to obtain a final reaction volume of 20 μL.

The reverse-transcription conditions were as follows: incubation at 37°C for 2 min, reverse transcription at 55°C for 15 min, enzyme inactivation at 85°C for 5 min, and holding at 4°C. The resulting cDNA was either used immediately for subsequent qPCR analysis or stored at − 20°C until use.

2.6 Real-Time Quantitative PCR

Real-time quantitative PCR (RT-qPCR) was performed to determine the relative expression levels of miR-15a-5p and the cell-cycle-related genes *CCND1*, *CCND2*, and *CDK6* in plasma and PBMC samples from the HC, LTBI, and ATB groups. miRNA expression was normalized using miR-16 and miR-93 as reference miRNAs, whereas mRNA expression was normalized using *GAPDH*. All primers were synthesized by Sangon Biotech Co., Ltd. (Shanghai, China).

2.6.1 qPCR Reaction Mixture and Cycling Conditions

RT-qPCR was performed using SYBR Premix Ex Taq™ II (Tli RNaseH Plus; RR820A, Takara, Japan) on a StepOnePlus Real-Time PCR System (Applied Biosystems, USA). Each sample was analyzed in technical triplicate. A no-template control was included in each experiment by replacing the cDNA template with RNase-free water to monitor potential contamination of the reaction mixture or experimental procedure.

The total qPCR reaction volume was 20 μL and consisted of 10.0 μL of 2× SYBR Premix Ex Taq II, 0.8 μL of forward primer (10 μmol/L), 0.8 μL of reverse primer (10 μmol/L), 0.4 μL of 50× ROX Reference Dye II, 2.0 μL of cDNA template, and 6.0 μL of RNase-free water. The amplification program consisted of an initial denaturation step at 95°C for 30 s, followed by 40 cycles of denaturation at 95°C for 5 s and annealing/extension at 60°C for 30 s. Melting-curve analysis was performed after amplification to verify the specificity of the PCR products.

2.6.2 RT-qPCR Data Processing

Cycle threshold (Ct) values were obtained using the instrument software. The mean Ct value from three technical replicates was used for subsequent analysis. When marked variation was observed among technical replicates, or when abnormal amplification curves or non-specific melting-curve peaks were detected, the abnormal well was excluded, or the assay was repeated to ensure the reliability and reproducibility of the results.

For miRNA analysis, the mean Ct value of miR-16 and miR-93 was used as the reference Ct value for each sample and was subsequently used to calculate ΔCt. GAPDH was used as the reference gene for mRNA normalization. Relative expression levels were calculated using the $2^{-\Delta\Delta Ct}$ method. The mean ΔCt value of the HC group was used as the calibrator for relative-expression analysis.

2.7 Measurement of Plasma CRP and IL-6

CRP and IL-6 concentrations were measured using routine clinical laboratory platforms in the Department of Laboratory Medicine at Guilin People's Hospital. CRP was measured by immunoturbidimetry using a Cobas C702 automated clinical chemistry analyzer and the corresponding Roche CRP reagents (Roche Diagnostics, Mannheim, Germany). IL-6 was measured using a Cobas E601 electrochemiluminescence immunoassay analyzer and the corresponding Roche IL-6 assay kit (Roche Diagnostics, Mannheim, Germany).

All measurements were performed according to the manufacturers' instructions and the laboratory's standard operating procedures. The corresponding calibrators and quality-control materials were used for calibration and internal quality control, and all quality-control results were within the acceptable ranges. CRP and IL-6 concentrations were expressed as mg/L and pg/mL, respectively, and were used in subsequent statistical analyses.

2.8 Bioinformatics and Public Dataset Analyses

Publicly available tuberculosis-related datasets were obtained from the National Center for Biotechnology Information Gene Expression Omnibus (GEO) database to evaluate miR-15a-5p and the selected cell-cycle-related genes externally. The plasma exosomal miRNA dataset GSE116542 and the PBMC miRNA dataset GSE207244 were analyzed to assess miR-15a-5p expression and diagnostic performance. For GSE116542, the pulmonary tuberculosis subset comprising seven patients with pulmonary tuberculosis and eight healthy controls was included in the analysis. GSE207244 included five patients with tuberculosis and five control participants. The PBMC microarray dataset GSE62525, comprising seven participants in each of the HC, LTBI, and ATB groups, was analyzed to evaluate the expression patterns of *CCND1*, *CCND2*, and *CDK6*.

GEO data, platform annotations, and corresponding phenotype information were downloaded and organized using the GEOquery package in R. For microarray datasets, target miRNAs and genes were matched using the corresponding platform annotation files. When multiple probes mapped to the same gene, a representative probe was selected according to probe annotation, expression intensity, and signal stability. In GSE62525, technical replicates from the same participant were averaged before

participant-level analysis. Because the datasets differed in biological source, detection platform, and participant composition, they were analyzed independently and were not merged across studies.

The monocyte RNA-sequencing dataset GSE185372 was further analyzed to examine the cell-subset-specific expression of *CCND1*, *CCND2*, and *CDK6*. The dataset included 294 monocyte-subset RNA-sequencing libraries from 52 participants. Classical ($CD14^{+}CD16^{-}$), intermediate ($CD14^{+}CD16^{+}$), and non-classical ($CD14^{-}CD16^{+}$) monocytes were analyzed separately across TB-negative, LTBI, ATB baseline, and ATB post-treatment groups. Raw read counts were normalized using the trimmed mean of M-values method implemented in edgeR, and $\log_2$ counts per million ($\log_2$CPM) values were calculated using a prior count of 0.5.

Because multiple monocyte subsets were obtained from the same participants and patients with ATB contributed repeated baseline and post-treatment samples, cross-sectional comparisons were restricted to the independent TB-negative, LTBI, and ATB baseline groups within each monocyte subset. Treatment-related changes were evaluated using paired baseline and follow-up samples from the same participants. For subset-level ROC analyses, ATB baseline was designated as the positive outcome. When reduced expression indicated ATB, the ROC direction was specified accordingly so that AUC values were reported on a scale from 0.5 to 1.0.

2.9 Statistical Analysis

Statistical analyses and graphical presentation were performed using GraphPad Prism version 11.0, SPSS version 31.0, and R software. Normally distributed continuous variables are presented as the mean ± standard deviation and were compared using ordinary one-way analysis of variance, Welch's analysis of variance, or the independent-samples *t*-test, as appropriate. Non-normally distributed variables are presented as the median (interquartile range) and were analyzed using the Kruskal–Wallis test, Mann–Whitney *U* test, or Wilcoxon signed-rank test for paired data. Categorical variables are presented as *n* (%) and were compared using the chi-square test or Fisher's exact test. Appropriate post hoc comparisons were performed following significant overall three-group tests.

Relative expression levels were calculated using the $2^{-\Delta\Delta Ct}$ method, with miR-16 and miR-93 used for miRNA normalization and *GAPDH* used for mRNA normalization. The $2^{-\Delta\Delta Ct}$ values were $\log_2$-transformed before parametric analyses, whereas untransformed values are presented in the tables and figures. ROC curve analysis was performed to evaluate the discrimination of LTBI from HC, ATB from HC, and ATB from LTBI. AUCs with 95% confidence intervals, optimal cutoff values, sensitivity, and specificity were calculated, with cutoff values determined using the Youden index.

A multivariable binary logistic regression model was constructed to combine $\log_2$-transformed plasma miR-15a-5p, CRP, and IL-6 to distinguish ATB from LTBI, with ATB coded as 1 and LTBI as 0. Adjusted odds ratios and 95% confidence intervals were calculated, and multicollinearity was assessed using variance inflation factors. The AUC of the combined model was compared with those of the individual biomarkers using DeLong's test, with Benjamini–Hochberg adjustment for multiple comparisons.

Internal validation was performed using 1,000 bootstrap resamples to estimate optimism-corrected AUCs and 95% confidence intervals. Public dataset comparisons were performed using the Wilcoxon rank-sum test, the Kruskal–Wallis test, or the paired Wilcoxon signed-rank test, as appropriate. All tests were two-sided, and $P < 0.05$ was considered statistically significant.

3. Results

3.1. Baseline Characteristics of the Study Participants

A total of 150 participants were enrolled, including 50 patients with active tuberculosis (ATB), 50 individuals with latent tuberculosis infection (LTBI), and 50 healthy controls (HCs). The age, sex, and major clinical characteristics of the three groups are summarized in Table 1. No significant difference in age distribution was observed among the three groups. The median ages were 56 (52–62) years in the ATB group, 58 (54–65) years in the LTBI group, and 58 (52–67) years in the HC group ($P = 0.293$). The sex distribution was also comparable among the groups ($P = 0.759$).

With respect to diagnostic and clinical characteristics, all participants in the ATB and LTBI groups were IGRA-positive, whereas all HCs were IGRA-negative. All patients in the ATB group showed chest imaging findings consistent with active pulmonary tuberculosis, and 42 patients had positive sputum smear results. Symptoms including cough or sputum production, hemoptysis, and fever or night sweats were significantly more frequent in the ATB group than in the LTBI group (all $P < 0.001$). These findings were consistent with the clinical diagnostic characteristics of ATB, LTBI, and HC participants.

Table 1
Baseline characteristics and diagnostic features of participants in the ATB, LTBI, and HC groups

Characteristic	ATB(*n* = 50)	LTBI(*n* = 50)	HC(*n* = 50)	*P* value
Age, years	56(52,62)	58(54,65)	58(52,67)	0.293
Sex(male/female)	35/15	32/18	35/15	0.759
IGRA-positive, n (%)	50(100)	50(100)	0(0)	-
Positive chest imaging, n (%)	50(100)	0(0)	0(0)	-
Positive sputum smear, n (%)	42(84)	0(0)	0(0)	-
Previous anti-TB treatment	None	None	None	-
Smoking history, n (%)	26(52)	25(50)	25(50)	0.974
Diabetes mellitus, n (%)	8(16)	9(18)	8(16)	0.954
Hypertension, n (%)	16(32)	17(34)	16(32)	0.970
Expectoration, n (%)	45(90)	3(6)	/	< 0.001
Hemoptysis, n (%)	22(44)	0(0)	/	< 0.001
Fever/night sweats, n (%)	48(96)	2(4)	/	< 0.001

[1] Data for age are presented as the median (interquartile range) and were compared using the Kruskal–Wallis test. Categorical variables are presented as n (%) and were compared using the chi-square test or Fisher's exact test, as appropriate. $P < 0.05$ was considered statistically significant. IGRA, interferon-gamma release assay; ATB, active tuberculosis; LTBI, latent tuberculosis infection; HC, healthy control.

3.2. Expression of miR-15a-5p and Cell-Cycle-Related Genes in Plasma and PBMCs

To validate the expression patterns of the candidate miRNA and related cell-cycle genes across different tuberculosis infection states, RT-qPCR was performed to measure the relative expression levels of miR-15a-5p, CCND1, CCND2, and CDK6 in plasma and peripheral blood mononuclear cells (PBMCs). The plasma inflammatory markers C-reactive protein (CRP) and interleukin-6 (IL-6) were also measured.

In plasma, miR-15a-5p expression differed significantly among the three groups ($P < 0.0001$), with markedly higher levels in the ATB group than in the HC and LTBI groups. Plasma CRP and IL-6 concentrations were also significantly elevated in the ATB group (both $P < 0.0001$), indicating a more pronounced systemic inflammatory response in patients with ATB. In contrast, Plasma *CCND1*, *CCND2*, and *CDK6* expression did not differ significantly among the three groups (Table 2 and Fig. 1A).

Because cell-cycle-related genes are predominantly expressed in nucleated cells, their expression was further examined in PBMCs. PBMC miR-15a-5p showed an increasing trend in the LTBI and ATB groups, but the overall difference among the three groups was not statistically significant ($P = 0.1718$). The magnitude of the between-group variation was smaller than that observed in plasma.

Notably, CCND1 and CCND2 expression in PBMCs differed significantly among the three groups (both $P < 0.0001$). CCND1 expression was markedly lower in the LTBI and ATB groups than in the HC group, whereas CCND2 expression was elevated in both the LTBI and ATB groups, with the highest level observed in the LTBI group. No significant difference in PBMC CDK6 expression was observed among the three groups (Table 3 and Fig. 1B).

Table 2
Plasma biomarker levels in the HC, LTBI, and ATB groups

Biomarkers	**HC(*n* = 50)**	**LTBI(*n* = 50)**	**ATB(*n* = 50)**	***P***
miR-15a-5p	1.98 ± 2.47	3.16 ± 3.74	8.13 ± 9.16	< 0.0001
CCND1	3.28 ± 5.14	2.42 ± 3.58	1.85 ± 1.99	0.168
CCND2	1.40 ± 0.99	1.73 ± 1.61	1.26 ± 0.83	0.139
CDK6	1.71 ± 1.90	1.43 ± 1.51	1.71 ± 1.90	0.709
CRP, mg/L	4.67 ± 2.40	5.80 ± 2.48	24.00 ± 25.45	< 0.0001
IL-6, pg/mL	5.16 ± 2.39	5.60 ± 2.61	28.46 ± 31.00	< 0.0001

[1] Relative expression levels were calculated using the $2^{-\Delta\Delta Ct}$ method. Data are presented as the mean ± standard deviation. Statistical comparisons were performed using $\log_2$-transformed data. One-way analysis of variance was used for comparisons among the three groups, and Welch's analysis of variance was used when the assumption of homogeneity of variance was not met. $P < 0.05$ was considered statistically significant.

Table 3
PBMC biomarker expression levels in the HC, LTBI, and ATB groups

Biomarkers	**HC(*n* = 50)**	**LTBI(*n* = 50)**	**ATB(*n* = 50)**	***P***
miR-15a-5p	1.61 ± 1.58	2.11 ± 2.71	2.52 ± 2.76	0.172
CCND1	1.11 ± 0.51	0.47 ± 0.33	0.32 ± 0.35	< 0.0001
CCND2	1.13 ± 0.60	4.96 ± 2.11	3.25 ± 3.14	< 0.0001
CDK6	1.62 ± 1.72	2.11 ± 1.32	1.74 ± 1.41	0.247

(A) Relative expression levels of miR-15a-5p, CCND1, CCND2, and CDK6 in plasma samples from healthy controls (HCs), individuals with LTBI, and patients with ATB. (B) Relative expression levels of the

corresponding biomarkers in PBMCs. Relative expression levels were calculated using the $2^{-\Delta\Delta Ct}$ method. Data are presented as the mean ± standard deviation.

*P < 0.05, **P < 0.001, ***P < 0.0001; ns, not significant.

3.3. Diagnostic Performance of Plasma and PBMC Biomarkers

Receiver operating characteristic (ROC) curve analysis was performed to evaluate the ability of the candidate biomarkers to distinguish among different tuberculosis infection states.In plasma, the biomarkers showed limited ability to distinguish LTBI from HC (Table 4 and Fig. 2A). miR-15a-5p had the highest AUC, 0.652, followed by CRP at 0.647. The AUC values for IL-6, CCND1, CCND2, and CDK6 were close to 0.5, indicating limited discriminative power for LTBI.

For distinguishing ATB from HC, plasma miR-15a-5p showed good diagnostic performance, with an AUC of 0.846 (Fig. 2B). Its diagnostic performance was comparable to that of CRP and IL-6, which yielded AUC values of 0.836 and 0.829, respectively. CRP and IL-6 showed relatively high sensitivity but lower specificity than miR-15a-5p. In contrast, plasma CCND1, CCND2, and CDK6 showed limited discriminative ability, with AUCs of 0.505, 0.530, and 0.522, respectively.

In the direct comparison between ATB and LTBI, plasma IL-6 showed the highest discriminatory performance, with an AUC of 0.793, followed by CRP and miR-15a-5p, with AUC values of 0.756 and 0.740, respectively (Fig. 2C). Plasma CCND1, CCND2, and CDK6 showed limited discriminative ability, with AUCs of 0.553, 0.535, and 0.537, respectively. These results indicated that plasma miR-15a-5p, CRP, and IL-6 provided moderate discrimination between ATB and LTBI when evaluated individually.

In PBMCs, the cell-cycle-related genes showed stronger discriminatory performance for distinguishing LTBI from HC (Fig. 2D). CCND2 and CCND1 yielded AUC values of 0.904 and 0.866, respectively. PBMC miR-15a-5p showed moderate discriminatory performance, with an AUC of 0.667, whereas CDK6 showed limited performance, with an AUC of 0.570.

To distinguish ATB from HC, PBMC CCND1 showed the highest diagnostic performance, with an AUC of 0.908, followed by CCND2 at 0.756 (Fig. 2E). PBMC miR-15a-5p and CDK6 showed relatively weak discriminative performance, with AUCs of 0.629 and 0.552, respectively.

For the direct discrimination of ATB from LTBI, PBMC CCND2 showed the highest AUC of 0.724, followed by CCND1 at 0.675 (Fig. 2F). The corresponding AUC values for CDK6 and miR-15a-5p were 0.604 and 0.570, respectively. Collectively, plasma miR-15a-5p showed potential value for identifying ATB relative to HC, whereas PBMC CCND1 and CCND2 showed good performance in distinguishing tuberculosis infection states from HC. However, the individual biomarkers showed only a moderate or limited ability to distinguish ATB from LTBI directly.

Table 4
Diagnostic performance of key plasma and PBMC biomarkers for pairwise discrimination among the HC, LTBI, and ATB groups

Sample type	Diagnostic comparison	Markes	AUC	95%CI	Youden index	Sensitivity%	Specificity%
plasma	ATB vs HC	miR-15a-5p	0.846	0.773–0.920	0.64	86	78
plasma	ATB vs HC	*CRP*	0.836	0.759–0.912	0.56	92	64
plasma	ATB vs HC	*IL-6*	0.829	0.749–0.908	0.46	90	56
PBMC	LTBI vs HC	*CCND1*	0.866	0.798–0.935	0.58	84	74
PBMC	LTBI vs HC	*CCND2*	0.904	0.843–0.976	0.80	82	98
PBMC	ATB vs HC	*CCND1*	0.908	0.852–0.964	0.68	72	96
PBMC	ATB vs HC	*CCND2*	0.756	0.658–0.854	0.54	66	88
Plasma	ATB vs LTBI	*miR-15a-5p*	0.740	0.644–0.836	0.44	48	96
Plasma	ATB vs LTBI	*CRP*	0.756	0.662–0.850	0.50	50	100
Plasma	ATB vs LTBI	*IL-6*	0.793	0.706–0.881	0.50	56	94
PBMC	ATB vs LTBI	*CCND1*	0.675				
PBMC	ATB vs LTBI	*CCND2*	0.724				

[1] AUC, area under the receiver operating characteristic curve; CI, confidence interval; HC, healthy control; LTBI, latent tuberculosis infection; ATB, active tuberculosis; PBMC, peripheral blood mononuclear cell; CRP, C-reactive protein; IL-6, interleukin-6.

Receiver operating characteristic (ROC) curve analyses were performed to evaluate the discriminatory performance of candidate biomarkers in plasma and peripheral blood mononuclear cells (PBMCs). (A) Plasma biomarkers for distinguishing individuals with latent tuberculosis infection (LTBI) from healthy controls (HCs). (B) Plasma biomarkers for distinguishing patients with active tuberculosis (ATB) from HCs. (C) Plasma biomarkers for distinguishing ATB from LTBI. (D) PBMC biomarkers for distinguishing LTBI from HCs. (E) PBMC biomarkers for distinguishing ATB from HCs. (F) PBMC biomarkers for distinguishing ATB from LTBI. Area under the ROC curve (AUC) values are shown in the corresponding panels. The diagonal line represents chance-level discrimination. HC, healthy control; LTBI, latent

tuberculosis infection; ATB, active tuberculosis; PBMC, peripheral blood mononuclear cell; ROC, receiver operating characteristic; AUC, area under the ROC curve.

3.4. Combined Plasma Biomarker Model for Distinguishing ATB from LTBI

To improve the direct discrimination of active tuberculosis (ATB) from latent tuberculosis infection (LTBI), a multivariable logistic regression model combining log_2-transformed plasma miR-15a-5p, CRP, and IL-6 was constructed. All three biomarkers remained independently associated with ATB after mutual adjustment. For each one-unit increase in the log_2-transformed value, the adjusted odds ratios were 2.303 for miR-15a-5p (95% CI, 1.545–3.804; $P < 0.001$), 2.742 for CRP (95% CI, 1.322–7.613; $P = 0.021$), and 2.977 for IL-6 (95% CI, 1.593–7.131; $P = 0.003$). No evidence of multicollinearity was observed among the predictors, with all variance inflation factors below 1.15 (Table 5).

The combined model achieved an apparent AUC of 0.920 (95% CI, 0.865–0.975), which was significantly higher than the AUCs of plasma miR-15a-5p (0.740), CRP (0.756), and IL-6 (0.793) individually. DeLong's test showed significant differences between the combined model and each biomarker after Benjamini–Hochberg correction for multiple comparisons (all adjusted $P < 0.001$).

Internal validation using 1,000 bootstrap resamples yielded a corrected AUC of 0.913 (95% CI, 0.866–0.976), corresponding to an optimism estimate of 0.007. The bootstrap-corrected AUCs of miR-15a-5p, CRP, and IL-6 were 0.742, 0.757, and 0.794, respectively. At the optimal cutoff, the combined model achieved a sensitivity of 90%, a specificity of 86%, and an overall accuracy of 88%. These findings indicated that combining plasma miR-15a-5p with CRP and IL-6 substantially improved the discrimination between ATB and LTBI compared with individual biomarkers (Fig. 3).

Table 5
Multivariable logistic regression analysis of plasma biomarkers for distinguishing ATB from LTBI

Predictor	β coefficient	Adjusted OR	95% CI	*P* value
Plasma miR-15a-5p	0.834	2.303	1.545–3.804	< 0.001
CRP	1.009	2.742	1.322–7.613	0.021
IL-6	1.091	2.977	1.593–7.131	0.003

(A) Receiver operating characteristic (ROC) curves for plasma miR-15a-5p, C-reactive protein (CRP), interleukin-6 (IL-6), and the three-biomarker combined model for distinguishing active tuberculosis (ATB) from latent tuberculosis infection (LTBI). The combined model was constructed using multivariable logistic regression with log_2-transformed biomarker values. Apparent areas under the ROC curve (AUCs) are shown in the legend, and the diagonal line represents chance-level discrimination. (B) Bootstrap-corrected AUCs and 95% confidence intervals based on 1,000 bootstrap resamples. Squares represent the corrected AUC estimates, horizontal lines represent the corresponding 95% confidence intervals, and

the vertical dashed line indicates an AUC of 0.5. Pairwise comparisons between the apparent AUC of the combined model and those of the individual biomarkers were performed using DeLong's test with Benjamini–Hochberg adjustment for multiple comparisons; all adjusted *P* values were < 0.001. AUC, area under the ROC curve; CI, confidence interval; CRP, C-reactive protein; IL-6, interleukin-6; ATB, active tuberculosis; LTBI, latent tuberculosis infection.

3.5. External Evaluation of Candidate Biomarkers in Public Tuberculosis Datasets

To externally evaluate the candidate biomarkers, GSE116542 and GSE207244 were analyzed for miR-15a-5p, whereas GSE62525 was analyzed for the PBMC cell-cycle-related genes *CCND1*, *CCND2*, and *CDK6*. The datasets were analyzed independently because of differences in sample source, detection platform, and clinical composition.

In the plasma exosomal miRNA dataset GSE116542, miR-15a-5p expression was significantly higher in patients with pulmonary tuberculosis than in healthy controls (Wilcoxon rank-sum test, $P = 0.014$), with an AUC of 0.884. In contrast, the PBMC miRNA dataset GSE207244 showed no significant difference in miR-15a-5p expression between patients with tuberculosis and controls ($P = 0.400$), and the corresponding AUC was 0.600. These findings were consistent with the significant elevation of plasma miR-15a-5p and the non-significant PBMC result observed in the present clinical cohort (Fig. 4).

GSE62525 included seven participants in each of the HC, LTBI, and ATB groups. Technical replicates from the same participant were averaged before analysis. *CCND1* showed a decreasing trend across the HC, LTBI, and ATB groups, although the overall difference was not statistically significant (Kruskal–Wallis $P = 0.180$). *CCND2* differed significantly among the three groups ($P = 0.030$), whereas *CDK6* showed no significant differences among groups ($P = 0.420$). ROC analysis showed that *CCND2* yielded AUCs of 0.816 for LTBI versus HC, 0.898 for ATB versus HC, and 0.429 for ATB versus LTBI. *CCND1* yielded an AUC of 0.755 for LTBI versus HC, whereas *CDK6* showed limited discriminatory performance across the three comparisons. The decreasing trend in *CCND1* and the non-significant *CDK6* result were generally consistent with the present PBMC findings, whereas the expression pattern of *CCND2* was not fully concordant (Fig. 5).

(A–C) Boxplots showing the expression levels of CCND1, CCND2, and CDK6 in peripheral blood mononuclear cells (PBMCs) from healthy controls (HCs), individuals with latent tuberculosis infection (LTBI), and patients with active tuberculosis (ATB) in GSE62525. Group differences were assessed using the Kruskal–Wallis test. (D–F) Receiver operating characteristic (ROC) curve analysis of CCND1, CCND2, and CDK6 for distinguishing LTBI from HC, ATB from HC, and ATB from LTBI. AUC values are shown in the corresponding panels.

*HC, healthy control; LTBI, latent tuberculosis infection; ATB, active tuberculosis; PBMC, peripheral blood mononuclear cell; ROC, receiver operating characteristic; AUC, area under the ROC curve.

3.6. Monocyte Subset-Specific Expression and Diagnostic Performance of Cell-Cycle-Related Genes in GSE185372

To further investigate the cellular basis of the PBMC findings, we analyzed the monocyte RNA-sequencing dataset GSE185372, which included 294 sequencing libraries from 52 participants. Classical ($CD14^{+}CD16^{-}$), intermediate ($CD14^{+}CD16^{+}$), and non-classical ($CD14^{-}CD16^{+}$) monocytes were analyzed separately across TB-negative, LTBI, ATB baseline, and ATB post-treatment groups. Comparisons among disease groups were restricted to TB-negative, LTBI, and ATB baseline samples, whereas paired baseline and post-treatment samples were used to assess longitudinal changes.

The three genes showed distinct monocyte subset-specific expression patterns (Fig. 6A). *CCND1* expression remained close to the lower detection limit in most monocyte subsets and disease groups, suggesting that the marked reduction observed in bulk PBMCs in our clinical cohort was unlikely to originate predominantly from circulating monocytes. *CCND2* was most highly expressed in non-classical monocytes, whereas *CDK6* showed relatively higher expression in intermediate and non-classical monocytes.

The strongest disease-associated signals were observed for *CCND2* in classical monocytes and *CDK6* in intermediate monocytes. In classical monocytes, *CCND2* expression was significantly lower in ATB baseline samples than in TB-negative and LTBI samples (Kruskal–Wallis $P < 0.001$). It distinguished ATB baseline from TB-negative and LTBI samples with AUCs of 0.88 and 0.89, respectively (Fig. 6B, C). In intermediate monocytes, *CDK6* expression also differed significantly among the three groups (Kruskal–Wallis $P < 0.001$), with lower expression in ATB baseline samples. The corresponding AUCs were 0.81 for ATB versus TB-negative and 0.78 for ATB versus LTBI. In contrast, *CCND1* showed limited discriminatory performance across all monocyte subsets.

Paired longitudinal analysis further showed that *CCND2* expression in classical monocytes increased after 2–3 months of anti-tuberculosis treatment. Among 20 paired participants, the median expression increased from 2.24 $\log_2$CPM at baseline to 3.35 $\log_2$CPM after treatment (paired Wilcoxon signed-rank test, $P = 0.026$), approaching the median levels observed in the TB-negative and LTBI groups (Fig. 6D). Twelve of the 20 participants showed increased expression after treatment. By contrast, *CDK6* expression in intermediate monocytes did not change significantly between baseline and follow-up ($P = 0.89$).

Overall, the GSE185372 analysis indicated that the cell-cycle-related signals observed in bulk PBMCs were strongly dependent on the immune cell subset. The absence of a clear *CCND1* signal in monocytes suggested a possible contribution from lymphocyte populations or changes in PBMC composition. The ATB-associated reduction of *CCND2* in classical monocytes, which increased after treatment, ran counter to the overall elevation observed in bulk PBMCs, highlighting substantial cell-subset heterogeneity. Similarly, the significant *CDK6* alteration in intermediate monocytes may have been

masked in bulk PBMC analysis. These findings provide cell-subset-level context for the clinical PBMC results rather than direct replication.

*TB-negative, tuberculosis-negative control; LTBI, latent tuberculosis infection; ATB, active tuberculosis; AUC, area under the receiver operating characteristic curve; log_2CPM, log_2 counts per million.

4. Discussion

MTB infection can remain latent for prolonged periods, and a proportion of individuals with LTBI may progress to ATB when host immune function declines or immune homeostasis is disrupted[20]. Because current diagnostic approaches remain limited in their ability to distinguish among different tuberculosis infection states, the identification of stable and readily measurable host-derived biomarkers remains an important priority [21]. Building on our previous discovery-stage plasma miRNA sequencing study[14], the present investigation evaluated miR-15a-5p and selected cell cycle–related genes in an expanded clinical cohort comprising patients with ATB, individuals with LTBI, and healthy controls. The principal findings were that plasma miR-15a-5p was significantly elevated in ATB, PBMC *CCND1* and *CCND2* showed marked but directionally distinct expression changes, and a plasma model combining miR-15a-5p, CRP, and IL-6 substantially improved the direct discrimination of ATB from LTBI. Public dataset analyses further demonstrated that these molecular signals were dependent on biological compartment and immune-cell subset, with classical-monocyte *CCND2* additionally showing a treatment-associated increase.

Previous studies have identified numerous tuberculosis-associated miRNAs in plasma, serum, whole blood, and extracellular vesicles, although the overlap among reported candidates has been limited[22, 23]. Such inconsistency likely reflects differences in sample type, disease stage, study population, detection platform, and data-processing strategy. In the present study, plasma miR-15a-5p was significantly higher in ATB than in both HC and LTBI. It showed good discrimination between ATB and HC (AUC 0.846) but only limited discrimination between LTBI and HC (AUC 0.652). These findings suggest that circulating miR-15a-5p is more closely associated with active disease than with MTB infection alone and may therefore be more suitable as an adjunctive marker of ATB than as a marker for identifying LTBI.

The public miRNA datasets supported this sample type–dependent pattern. In the plasma exosomal dataset GSE116542, miR-15a-5p was significantly elevated in pulmonary tuberculosis and yielded an AUC of 0.884, consistent with the plasma findings in our clinical cohort. In contrast, neither GSE207244 nor our clinical PBMC analysis demonstrated a significant difference in intracellular miR-15a-5p expression. Although reduced miR-15a-5p expression has been reported in another pulmonary tuberculosis study, the direction of circulating miRNA changes may vary depending on specimen type and analytical methodology [24]. Extracellular vesicles or protein complexes may carry plasma miRNAs and originate from circulating immune cells, infected tissues, cellular injury, or apoptosis [25]. Circulating levels therefore do not necessarily parallel intracellular expression in PBMCs. The elevation of plasma

miR-15a-5p in ATB may consequently represent a composite signal generated by infection-associated immune activation and tissue injury rather than a simple reflection of PBMC transcription.

A major finding of this study was that combining miR-15a-5p with conventional inflammatory markers markedly improved the direct discrimination of ATB from LTBI. When assessed individually, plasma miR-15a-5p, CRP, and IL-6 provided only moderate discrimination, with AUCs of 0.740, 0.756, and 0.793, respectively. In the multivariable model, however, all three biomarkers remained independently associated with ATB after adjustment for mutual confounding, and the combined model achieved an apparent AUC of 0.920. Its discriminatory performance was significantly greater than that of each biomarker according to DeLong's test after adjustment for multiple comparisons. At the optimal cutoff, the model achieved 90% sensitivity, 86% specificity, and 88% accuracy. These findings indicate that a circulating miRNA and conventional inflammatory markers may provide complementary diagnostic information rather than completely overlapping signals.

The model also showed favorable internal stability. After 1,000 bootstrap resamples, the optimism-corrected AUC remained 0.913, corresponding to an optimism estimate of only 0.007. The small reduction between apparent and corrected performance suggests that substantial overfitting was not evident within the present cohort. Nevertheless, bootstrap correction represents internal rather than external validation, and the model's performance may still vary across populations with different epidemiological backgrounds, comorbidities, or disease severity. Hence, the diagnostic efficacy of the combined model requires further validation with expanded sample sizes and diverse disease cohorts.

CRP and IL-6 were markedly elevated in ATB, consistent with their established roles as indicators of systemic inflammation. Their relatively lower specificity in the ATB-versus-HC comparison also accords with the fact that both markers can be elevated in other infections, malignancies, and autoimmune disorders[26, 27]. miR-15a-5p belongs to the miR-15/16 family and has been implicated in cell-cycle regulation, apoptosis, NF-κB-associated signaling, macrophage activation, and autophagy[11]. Its contribution to the combined model may therefore reflect molecular processes not fully captured by conventional inflammatory markers [28]. However, because the present study did not include controls for other pulmonary infections or inflammatory diseases, the disease specificity of miR-15a-5p and the combined model remains to be established. Consistent with this interpretation, a recent prospective study found that CRP was less accurate than blood RNA biomarkers for tuberculosis diagnosis, supporting its use as a complementary inflammatory marker rather than a standalone diagnostic indicator[29].

The principal PBMC findings were the downregulation of *CCND1* and upregulation of *CCND2* in both LTBI and ATB. *CCND1* showed strong discrimination between LTBI and ATB and HC, whereas *CCND2* achieved an AUC of 0.904 for LTBI versus HC. Nevertheless, their performance for directly distinguishing ATB from LTBI was more modest, with AUCs of 0.675 and 0.724, respectively. Thus, these genes may primarily reflect tuberculosis-associated immune-cell transcriptional alterations rather than serving as sufficiently

accurate standalone markers for differentiating active from latent infection. *CDK6* showed no significant difference in bulk PBMCs.

CCND1, *CCND2*, and *CDK6* are core components of the cyclin D–CDK4/6 axis that regulates G1/S cell-cycle progression and has increasingly recognized immunomodulatory functions[30]. In our previous study, they were identified as key cell cycle–related candidate genes through target prediction and protein–protein interaction analyses, with *CCND1* additionally predicted to be a potential direct target of miR-15a-5p [14]. The present clinical findings therefore extend the previous bioinformatic observations by demonstrating altered expression of *CCND1* and *CCND2* in human tuberculosis samples. However, the major miR-15a-5p signal was observed in plasma, whereas the major gene-expression changes were observed in PBMCs, and PBMC miR-15a-5p itself was not significantly altered. These findings suggest that circulating miR-15a-5p may predominantly reflect extracellular release from infected tissues or activated and injured cells rather than altered intracellular expression within PBMCs. More importantly, the absence of a significant PBMC miR-15a-5p change indicates that the observed alterations in *CCND1* and *CCND2* cannot currently be attributed to direct miR-15a-5p-mediated regulation and may instead reflect independent transcriptional responses or changes in PBMC composition.

Consistent with this compartment-specific interpretation, plasma *CCND1*, *CCND2*, and *CDK6* transcripts showed no significant group differences. As low-abundance cell-free RNAs, plasma mRNAs may be influenced by extracellular-vesicle release, cellular injury, degradation, and heterogeneous tissue sources. They may therefore not faithfully reflect transcriptional activity in circulating immune cells[31]. Accordingly, the PBMC measurements likely provide a more direct representation of tuberculosis-associated immune-cell transcriptional changes.

GSE62525 provided partial external support for the PBMC findings. *CCND1* showed a similar decreasing trend, and *CDK6* again showed no consistent group differences, whereas CCND2 expression direction was discordant with our RT-qPCR results despite some discriminatory ability. Given the small sample size, microarray-based measurement, and differences in cohort composition, these findings should be regarded as exploratory rather than confirmatory. The discordant *CCND2* pattern also highlighted the need to examine cell-subset-specific expression.

To further explore the cellular origin of the bulk PBMC signals, we analyzed monocyte subsets in GSE185372. *CCND1* expression remained close to the lower detection limit across monocyte subsets. It showed limited diagnostic performance, suggesting that the reduction observed in bulk PBMCs was unlikely to be driven predominantly by circulating monocytes. By contrast, *CCND2* and *CDK6* showed clear subset-specific changes. Classical-monocyte *CCND2* was reduced in ATB and distinguished ATB from TB-negative and LTBI samples with AUCs of 0.88 and 0.89, respectively, whereas intermediate-monocyte *CDK6* showed corresponding AUCs of 0.81 and 0.78. The absence of a significant *CDK6* difference in bulk PBMCs may therefore reflect dilution of a signal restricted to a relatively small cell subset.

The reduction of *CCND2* in classical monocytes differed from its overall elevation in bulk PBMCs, highlighting the influence of cell composition and subset-specific transcription. Because bulk PBMC measurements integrate signals from multiple lymphoid and monocyte populations, changes in one subset may be masked or outweighed by those in others. Thus, the bulk PBMC and monocyte-subset findings should be viewed as complementary rather than contradictory and underscore the need for cell-resolved validation.

Notably, classical-monocyte *CCND2* increased after 2–3 months of anti-tuberculosis treatment and shifted toward the levels observed in TB-negative and LTBI samples. Reduced cyclin D2 expression has previously been reported in severe pulmonary tuberculosis, while broader monocyte and blood transcriptomic abnormalities have been shown to diminish during treatment[32, 33]. Our finding extends these observations by identifying a specific treatment-associated change in CCND2 in classical monocytes.

Several limitations should be acknowledged. First, the clinical cohort was derived from a single center, and the diagnostic model was developed and internally validated using the same 100 participants with ATB and LTBI. Although bootstrap correction indicated limited optimism, independent external validation remains necessary. Second, the study included healthy controls but no disease-control groups with other pulmonary infections or inflammatory disorders, limiting assessment of tuberculosis specificity. Third, the public datasets differed in specimen type, platform, cohort structure, and sample size and therefore provided exploratory contextual evidence rather than definitive external validation. Fourth, PBMCs are heterogeneous, and the clinical cohort did not include sorted-cell or single-cell analyses to establish the precise cellular origin of the observed gene-expression changes. Fifth, protein expression and direct miRNA–target interactions were not experimentally evaluated. Finally, longitudinal observations were obtained only from the public monocyte dataset; the clinical cohort itself lacked serial sampling during treatment and long-term follow-up of LTBI progression.

In conclusion, the present study confirmed that plasma miR-15a-5p is elevated in ATB and provides diagnostic information complementary to CRP and IL-6. Combining the three plasma biomarkers substantially improved the direct discrimination of ATB from LTBI and retained high performance after bootstrap correction. PBMC *CCND1* and *CCND2* levels reflected tuberculosis-associated cell cycle–related transcriptional alterations, while monocyte subset analysis revealed substantial cellular heterogeneity and identified a treatment-associated increase in classical monocyte *CCND2*. These findings support the potential value of integrating circulating miRNAs, inflammatory markers, and cell-specific transcriptional signals for tuberculosis classification. Still, multicentre external validation and mechanistic studies remain necessary before clinical application.

5. Conclusions

Plasma miR-15a-5p was significantly elevated in ATB and, when combined with CRP and IL-6, substantially improved the discrimination of ATB from LTBI, with stable performance after bootstrap

correction. PBMC *CCND1* and *CCND2* showed tuberculosis-associated expression changes, while analyses of public datasets revealed substantial sample- and cell-subset-specific heterogeneity. These findings support the combined plasma biomarker model as a promising approach for tuberculosis classification, although multicentre external and longitudinal validation is required.

Abbreviations

ATB
active tuberculosis
CRP
C-reactive protein
GEO
Gene Expression Omnibus
IGRAs
interferon-gamma release assays
IL-6
interleukin-6
LTBI
latent tuberculosis infection
miRNAs
microRNAs
MTB
Mycobacterium tuberculosis
PBMCs
peripheral blood mononuclear cells
RT-qPCR
Real-time quantitative PCR
TB
Tuberculosis
TST
tuberculin skin test

Declarations

Acknowledgments: We appreciate the support of many people. We thank the Precision Medicine Laboratory Center and the Research Department of Guilin People's Hospital. We are also grateful for the contributions of sample donors.

Author Contributions: Conceptualization, X.C. and J.Y.; methodology, X.C.; software, J.Y.; validation, S.L., J.X. and J.B.; formal analysis, L.Z.; investigation, S.L.; resources, J.W.; data curation, J.Y.; writing—original draft preparation, J.Y.; writing—review and editing, L.Y.; visualization, S.L.; supervision, L.Y.; project

administration, X.C.; funding acquisition, X.C., J.Y. and H.Z. X.C. and L.Y. contributed equally to this work and share first authorship. All authors read and approved the final manuscript.

Funding: This study was supported by Open Research Fund of the Key Laboratory of Clinical Laboratory Diagnostics of Guangxi Higher Education Institutions (GXGXLCJYZDX2025005), the Natural Science Foundation of Guangxi Zhuang Autonomous Region (2025GXNSFHA069096, 2024GXNSFAA010025) and Guangxi Medical and Health Appropriate Technology Development and Promotion Application Project (S2018018).

Data Availability Statement: The public datasets analysed in this study are available in the NCBI Gene Expression Omnibus under accession numbers GSE116542, GSE207244, GSE62525, and GSE185372. The datasets generated during the current study are available from the corresponding authors upon reasonable request.

Ethics approval and consent to participate: This collection and operation of clinical samples was approved by the Ethics Committee of Guilin People's Hospital (Guangxi, China; Approval No. 2026002KY; 12 Jan 2026), and was performed in accordance with the Declaration of Helsinki. Written informed consent was obtained from all participants or their legal representatives prior to enrollment.

Competing Interests: The authors declare no competing interests.

References

1. Bergman A, Thomas T. Overview of the Epidemiology, Diagnosis, and Clinical Care Considerations for People Living with and at Risk for Tuberculosis in the United States. Nurs Clin North Am. 2025;60(3):491–506.
2. Geneva WHO. WHO's Global Tuberculosis Report2023. Switzerland: WHO; 2024.
3. Li LS, Yang L, Zhuang L, Ye ZY, Zhao WG, Gong WP. From immunology to artificial intelligence: revolutionizing latent tuberculosis infection diagnosis with machine learning. Mil Med Res. 2023;10(1):58.
4. Boom WH, Schaible UE, Achkar JM. The knowns and unknowns of latent Mycobacterium tuberculosis infection. J Clin Invest 2021, 131(3).
5. Malhotra AG, Lokhande L, Pakhare A, Soni P, Vishwakarma SP, Maurya AK, Singh J, Singh S. Diagnostic yield of Xpert MTB/RIF, Xpert MTB/RIF Ultra, and Truenat MTB assays on non-pulmonary samples from suspected cases of extra-pulmonary tuberculosis (EPTB). Eur J Clin Microbiol Infect Dis 2025.
6. Scherer J, Locketz M, Castelein S, Dunn R, Held M, Thienemann F. Evaluation of clinical, laboratory, radiographical and histopathological characteristics in patients with spinal tuberculosis in the context of HIV infection: An analysis of 52 patients from a South African tertiary hospital. S Afr Med J. 2024;114(11):e2065.

7. Esposito S, Campana BR, Arnesano GG, Principi N. Tuberculosis Skin Test for the Diagnosis of Pediatric Tuberculosis: Comparison with Tuberculin Skin Test and Interferon-Gamma Release Assays. Microorganisms 2026, 14(5).
8. Yue C, Geng X, Sun X, Liu J, Zhang D, Li L. Emerging blood-based diagnostic strategies for tuberculosis. Clin Chem Lab Med 2026.
9. Jumat MI, Sarmiento ME, Acosta A, Chin KL. Role of non-coding RNAs in tuberculosis and their potential for clinical applications. J Appl Microbiol 2023, 134(6).
10. Chadalawada S, Rathinam SR, Lalitha P, Kannan NB, Devarajan B. Detection of microRNAs expression signatures in vitreous humor of intraocular tuberculosis. Mol Biol Rep. 2023;50(12):10061–72.
11. Gonzalez-Lopez P, Alvarez-Villarreal M, Ruiz-Simon R, Lopez-Pastor AR, de Ceniga MV, Esparza L, Martin-Ventura JL, Escribano O, Gomez-Hernandez A. Role of miR-15a-5p and miR-199a-3p in the inflammatory pathway regulated by NF-kappaB in experimental and human atherosclerosis. Clin Transl Med. 2023;13(8):e1363.
12. Li Y, Li D, Yang Y, Wang J. miR-15a-5p Regulates Liver Cancer Cell Migration, Apoptosis and Cell Cycle Progression by Targeting Transcription Factor E2F3. Crit Rev Eukaryot Gene Expr. 2022;32(6):1–10.
13. Zhu QJ, Wang J, Li Y, Bai ZJ, Guo XB, Pan T. PRKCA Promotes Mitophagy through the miR-15a-5p/PDK4 Axis to Relieve Sepsis-Induced Acute Lung Injury. Infect Immun. 2023;91(1):e0046522.
14. Yang J, Dan H, Chen Y, Zou L, Liu S, Wang F, Musa MB. miRNA Differential Expression Profile Analysis and Identification of Potential Key Genes in Active Tuberculosis. J Cell Mol Med. 2025;29(10):e70567.
15. Petasny M, Bentata M, Pawellek A, Baker M, Kay G, Salton M. Splicing to Keep Cycling: The Importance of Pre-mRNA Splicing during the Cell Cycle. Trends Genet. 2021;37(3):266–78.
16. Qie S, Diehl JA. Cyclin D1, cancer progression, and opportunities in cancer treatment. J Mol Med (Berl). 2016;94(12):1313–26.
17. Zhao YX, Xu BW, Wang FQ, Jiang FY, Xu JW, Yu DX. nc-RNA-mediated high expression of CDK6 correlates with poor prognosis and immune infiltration in pancreatic cancer. Cancer Med. 2023;12(4):5110–23.
18. Li N, Zeng J, Sun F, Tong X, Meng G, Wu C, Ding X, Liu L, Han M, Lu C, et al. p27 inhibits CDK6/CCND1 complex formation resulting in cell cycle arrest and inhibition of cell proliferation. Cell Cycle. 2018;17(19–20):2335–48.
19. Jardim DL, Millis SZ, Ross JS, Woo MS, Ali SM, Kurzrock R. Cyclin Pathway Genomic Alterations Across 190,247 Solid Tumors: Leveraging Large-Scale Data to Inform Therapeutic Directions. Oncologist. 2021;26(1):e78–89.
20. Konjengbam BD, Meitei HN, Pandey A, Haobam R. Goals and strategies in vaccine development against tuberculosis. Mol Immunol. 2025;183:56–71.

21. Abdulhadi A, Abdullahi N, Yusuf I, Waziri BI, Mamuda K, Ibrahim HF, Muhammad K, Ibrahim MM, Abdullahi AA, Murtala HA, et al. A Systematic Review and Meta-analysis on Innovative Approaches in Tuberculosis Diagnosis: Challenges and Future Directions. Int J MCH AIDS. 2026;15:e006.
22. Gunasekaran H, Sampath P, Thiruvengadam K, Malaisamy M, Ramasamy R, Ranganathan UD, Bethunaickan R. A systematic review and meta-analysis of circulating serum and plasma microRNAs in TB diagnosis. BMC Infect Dis. 2024;24(1):402.
23. Sundaram K, Rathinam S. Advances in functional transcriptome analysis of Mycobacterium tuberculosis: a review. Mol Genet Genomics 2026, 301(1).
24. Cavusoglu C, Cogulu O, Durmaz A, Cengisiz Z, Yilmaz FF, Tasbakan MS, Tasbakan M, Gunduz C, Bicmen C, Karaman O, et al. Investigation of miRNA and cytokine expressions in latent tuberculosis infection and active tuberculosis. Turk J Med Sci. 2022;52(3):649–57.
25. Jingwen X, Shiyue M, Qiupei T, Jianlong X, Shanshan L, Qingfeng S, Jun Y. Diagnostic exosomal microRNAs and pathogenic regulatory networks in hepatocellular carcinoma revealed by exosomal RNA sequencing: A case-control study. J Int Med Res. 2026;54(1):3000605251411664.
26. Pepys MB, Hirschfield GM. C-reactive protein: a critical update. J Clin Invest. 2003;111(12):1805–12.
27. Hunter CA, Jones SA. IL-6 as a keystone cytokine in health and disease. Nat Immunol. 2015;16(5):448–57.
28. Peng H, Wang J, Li S. MiR-15a-5p accelerated vascular smooth muscle cells viabilities and migratory abilities via targeting Bcl-2. Physiol Res. 2022;71(5):667–75.
29. Mann T, Minnies S, Gupta RK, Reeve BWP, Nyawo G, Palmer Z, Naidoo C, Doubell A, Pecoraro A, John TJ, et al. Blood RNA biomarkers and C-reactive protein for triage of adult patients with tuberculosis lymphadenitis and pericarditis in South Africa: a single-centre, prospective, observational, diagnostic accuracy study. Lancet Microbe. 2025;6(9):101153.
30. Saleban M, Harris EL, Poulter JA. D-Type Cyclins in Development and Disease. Genes (Basel) 2023, 14(7).
31. De Sota RE, Quake SR, Sninsky JJ, Toden S. Decoding bioactive signals of the RNA secretome: the cell-free messenger RNA catalogue. Expert Rev Mol Med. 2024;26:e12.
32. Fan L, Shen H, Huang H, Yang R, Yao L. Impairment of Wnt/beta-catenin signaling in blood cells of patients with severe cavitary pulmonary tuberculosis. PLoS ONE. 2017;12(3):e0172549.
33. Hillman H, Khan N, Singhania A, Dubelko P, Soldevila F, Tippalagama R, DeSilva AD, Gunasena B, Perera J, Scriba TJ, et al. Single-cell profiling reveals distinct subsets of CD14 + monocytes drive blood immune signatures of active tuberculosis. Front Immunol. 2022;13:1087010.

Figures

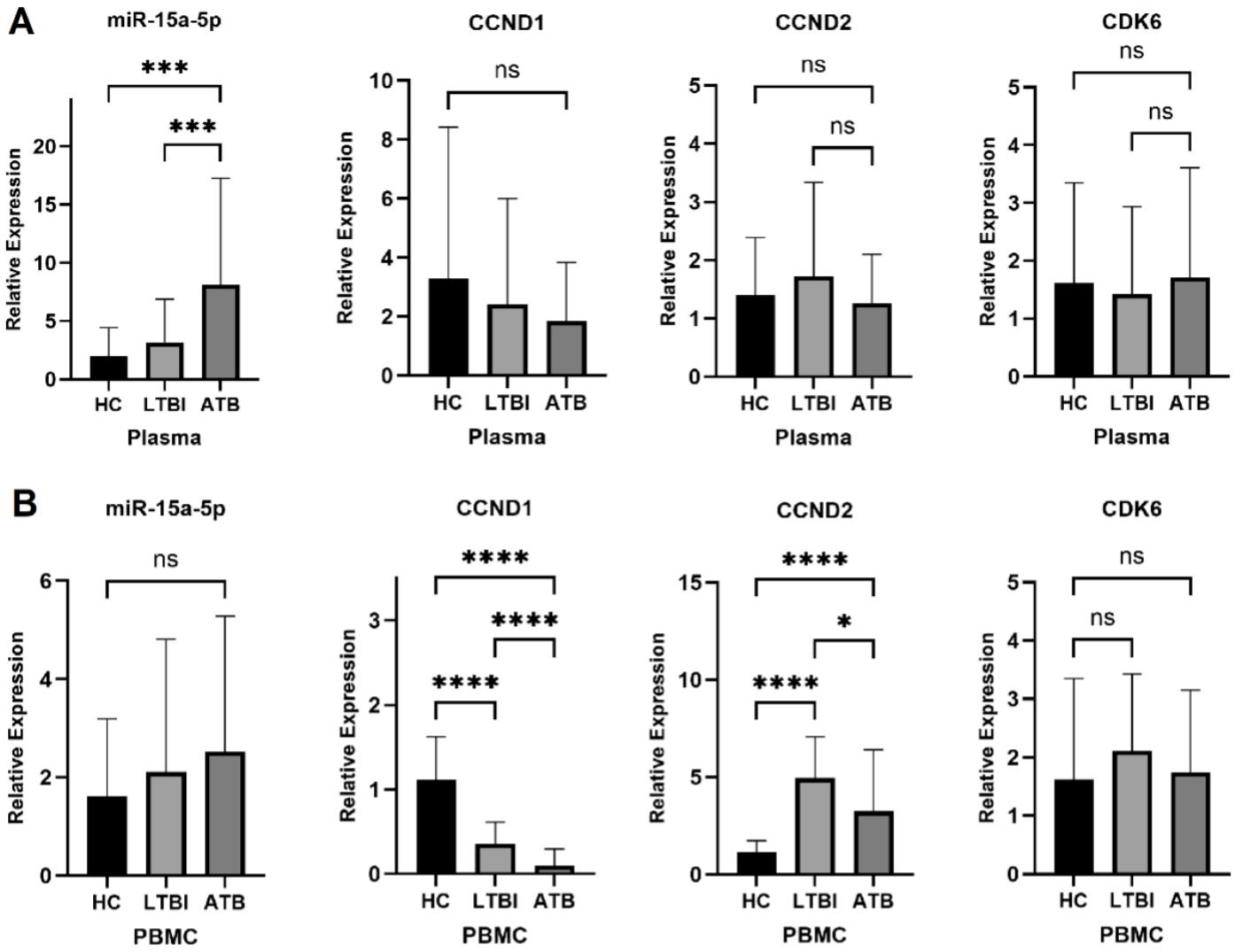

Figure 1

Relative expression levels of miR-15a-5p and cell-cycle-related genes in plasma and PBMCs

(A) Relative expression levels of miR-15a-5p, CCND1, CCND2, and CDK6 in plasma samples from healthy controls (HCs), individuals with LTBI, and patients with ATB. (B) Relative expression levels of the corresponding biomarkers in PBMCs. Relative expression levels were calculated using the $2^{-\Delta\Delta Ct}$ method. Data are presented as the mean ± standard deviation.
*P < 0.05, **P < 0.001, ***P < 0.0001; ns, not significant.

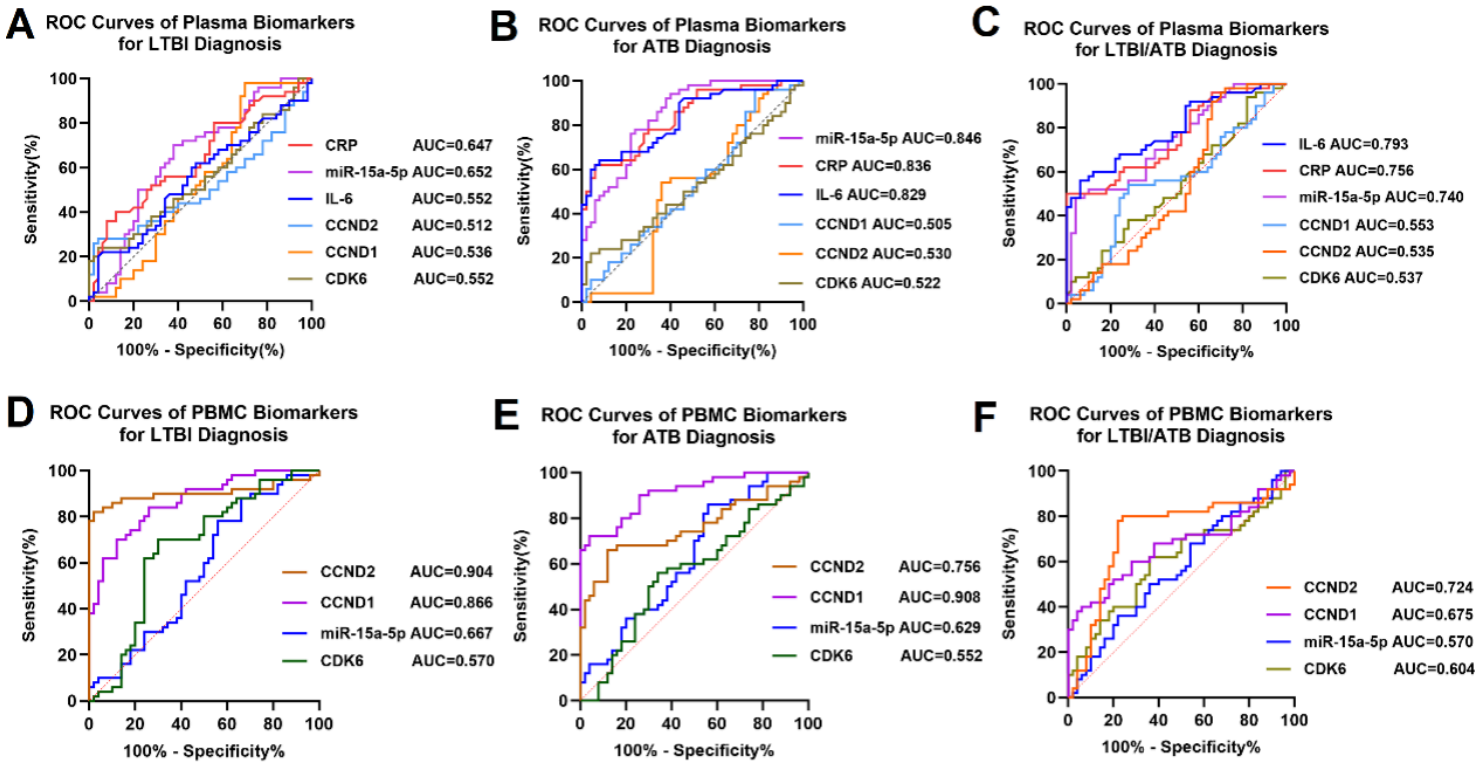

Figure 2

Diagnostic performance of plasma and PBMC biomarkers across different tuberculosis infection states.

Receiver operating characteristic (ROC) curve analyses were performed to evaluate the discriminatory performance of candidate biomarkers in plasma and peripheral blood mononuclear cells (PBMCs). (A) Plasma biomarkers for distinguishing individuals with latent tuberculosis infection (LTBI) from healthy controls (HCs). (B) Plasma biomarkers for distinguishing patients with active tuberculosis (ATB) from HCs. (C) Plasma biomarkers for distinguishing ATB from LTBI. (D) PBMC biomarkers for distinguishing LTBI from HCs. (E) PBMC biomarkers for distinguishing ATB from HCs. (F) PBMC biomarkers for distinguishing ATB from LTBI. Area under the ROC curve (AUC) values are shown in the corresponding panels. The diagonal line represents chance-level discrimination. HC, healthy control; LTBI, latent tuberculosis infection; ATB, active tuberculosis; PBMC, peripheral blood mononuclear cell; ROC, receiver operating characteristic; AUC, area under the ROC curve.

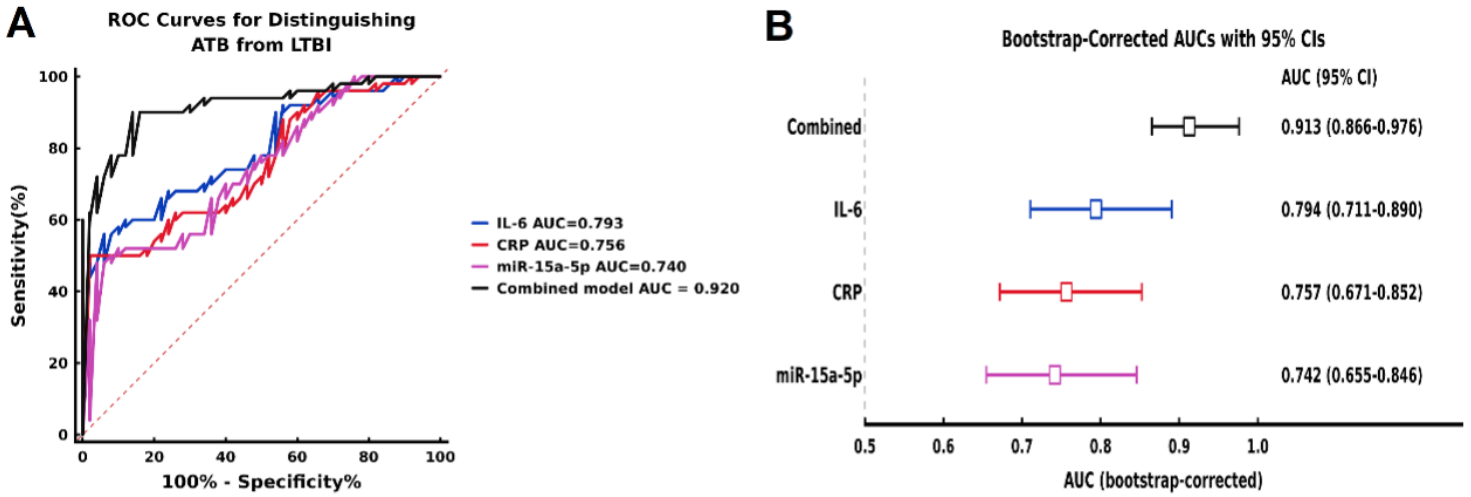

Figure 3

Diagnostic performance and bootstrap internal validation of the combined plasma biomarker model for distinguishing ATB from LTBI.

(A) Receiver operating characteristic (ROC) curves for plasma miR-15a-5p, C-reactive protein (CRP), interleukin-6 (IL-6), and the three-biomarker combined model for distinguishing active tuberculosis (ATB) from latent tuberculosis infection (LTBI). The combined model was constructed using multivariable logistic regression with $\log_2$-transformed biomarker values. Apparent areas under the ROC curve (AUCs) are shown in the legend, and the diagonal line represents chance-level discrimination. (B) Bootstrap-corrected AUCs and 95% confidence intervals based on 1,000 bootstrap resamples. Squares represent the corrected AUC estimates, horizontal lines represent the corresponding 95% confidence intervals, and the vertical dashed line indicates an AUC of 0.5. Pairwise comparisons between the apparent AUC of the combined model and those of the individual biomarkers were performed using DeLong's test with Benjamini–Hochberg adjustment for multiple comparisons; all adjusted *P* values were <0.001. AUC, area under the ROC curve; CI, confidence interval; CRP, C-reactive protein; IL-6, interleukin-6; ATB, active tuberculosis; LTBI, latent tuberculosis infection.

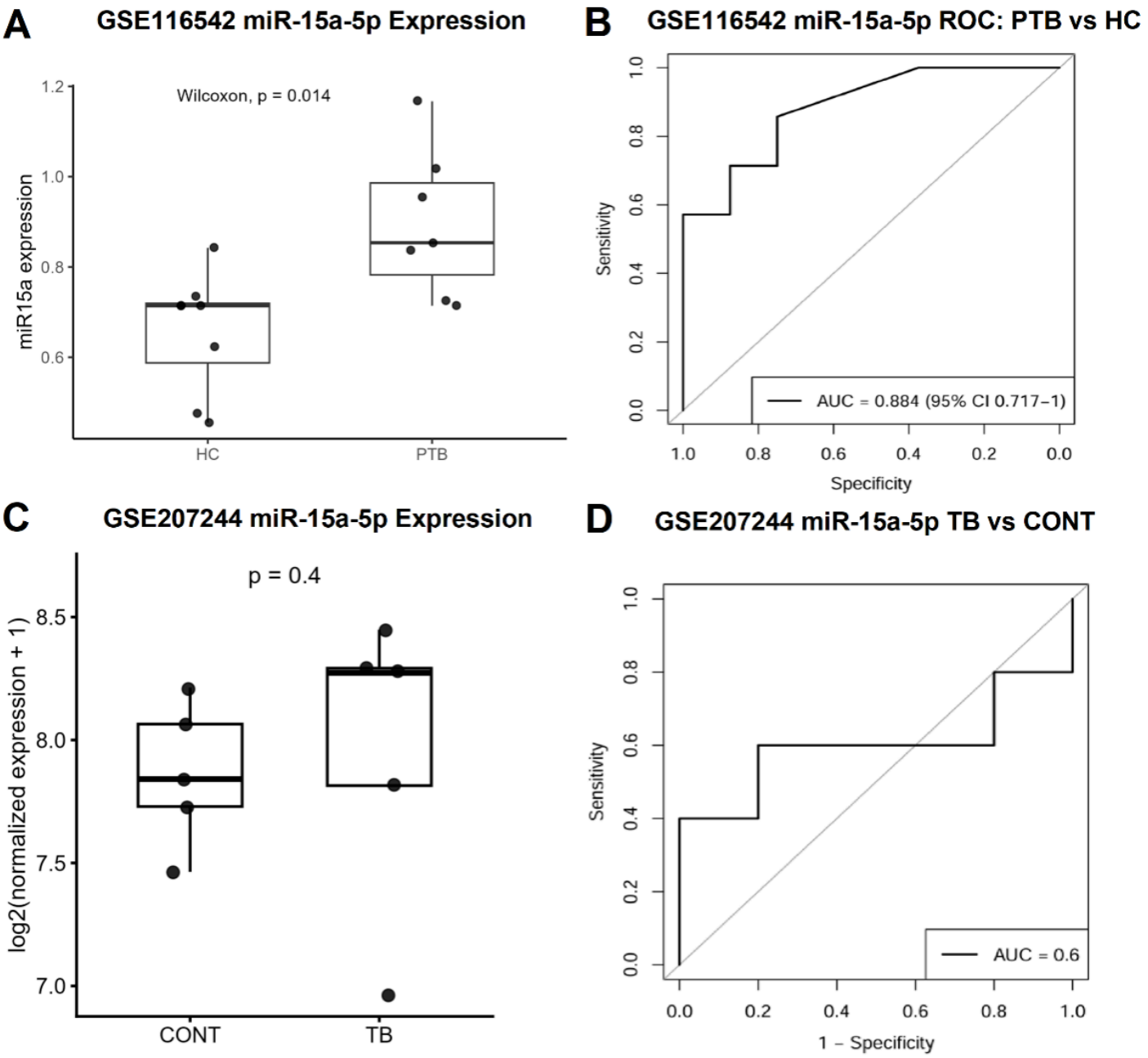

Figure 4

External evaluation of miR-15a-5p expression and diagnostic performance in public tuberculosis datasets. (A, B) Expression of miR-15a-5p and receiver operating characteristic (ROC) curve analysis for distinguishing patients with pulmonary tuberculosis (PTB) from healthy controls (HCs) in GSE116542. (C, D) Expression of miR-15a-5p and ROC curve analysis for distinguishing patients with tuberculosis (TB) from control participants (CONT) in GSE207244. Between-group differences were assessed using the Wilcoxon rank-sum test. *P*values and areas under the ROC curve (AUCs) are indicated in the corresponding panels. HC, healthy control; PTB, pulmonary tuberculosis; CONT, control; TB, tuberculosis; ROC, receiver operating characteristic; AUC, area under the ROC curve.

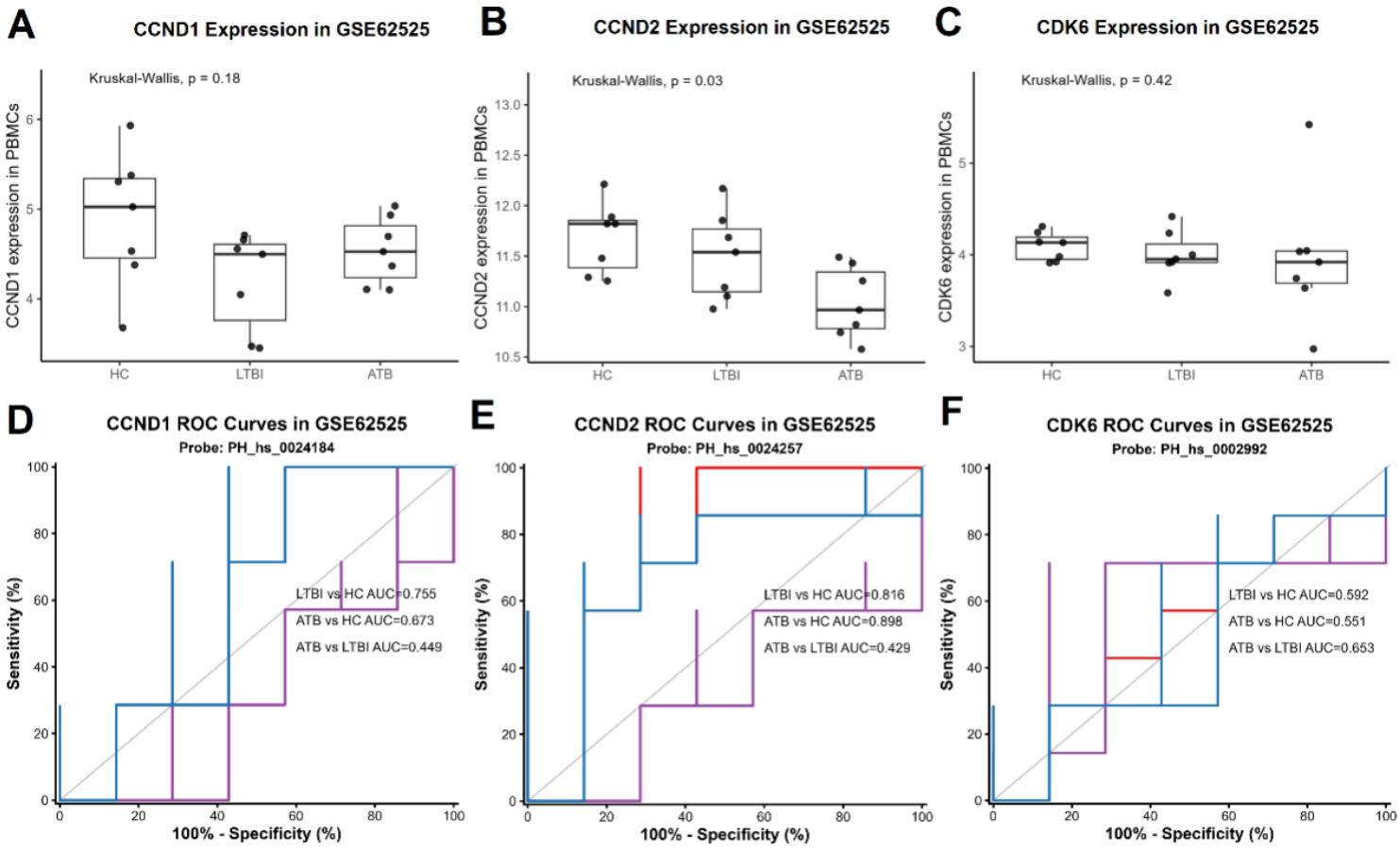

Figure 5

Expression patterns and diagnostic performance of CCND1, CCND2, and CDK6 in PBMCs from GSE62525

(A–C) Boxplots showing the expression levels of CCND1, CCND2, and CDK6 in peripheral blood mononuclear cells (PBMCs) from healthy controls (HCs), individuals with latent tuberculosis infection (LTBI), and patients with active tuberculosis (ATB) in GSE62525. Group differences were assessed using the Kruskal–Wallis test. (D–F) Receiver operating characteristic (ROC) curve analysis of CCND1, CCND2, and CDK6 for distinguishing LTBI from HC, ATB from HC, and ATB from LTBI. AUC values are shown in the corresponding panels.

*HC, healthy control; LTBI, latent tuberculosis infection; ATB, active tuberculosis; PBMC, peripheral blood mononuclear cell; ROC, receiver operating characteristic; AUC, area under the ROC curve.

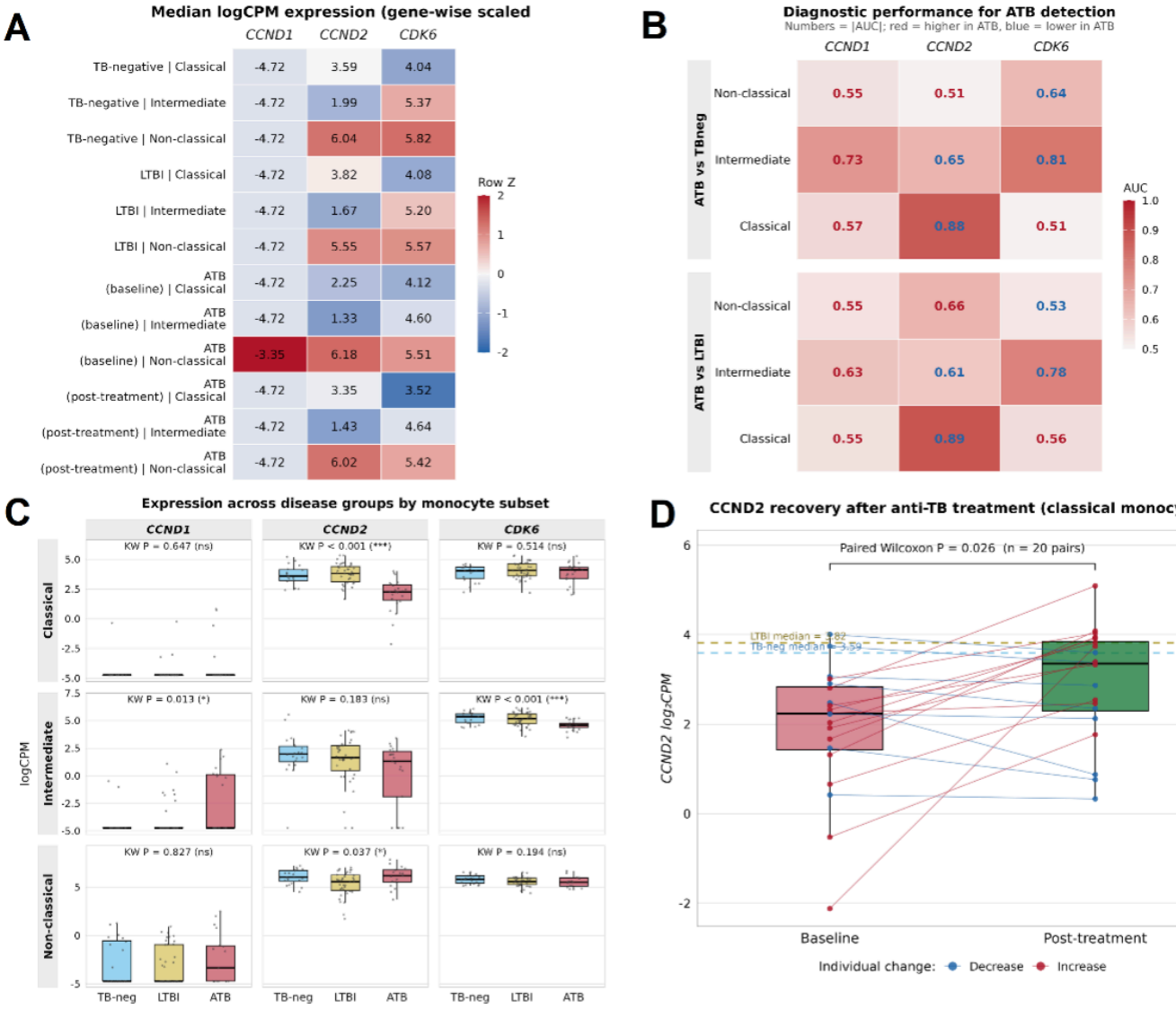

Figure 6

Cell-cycle-related gene expression and diagnostic performance across monocyte subsets in GSE185372. (A) Heatmap showing the median $\log_2$ counts per million ($\log_2$CPM) expression levels of CCND1, CCND2, and CDK6 across TB-negative, latent tuberculosis infection (LTBI), active tuberculosis (ATB) baseline, and ATB post-treatment groups in classical, intermediate, and non-classical monocytes. The color scale represents gene-wise standardized median expression. (B) Area under the receiver operating characteristic curve (AUC) values for distinguishing ATB baseline samples from TB-negative or LTBI samples across genes and monocyte subsets. Red values indicate higher expression in ATB, whereas blue values indicate lower expression in ATB.(C) Expression distributions of CCND1, CCND2, and CDK6 across TB-negative, LTBI, and ATB baseline groups within each monocyte subset. Group differences were assessed using the Kruskal–Wallis test.(D) Paired changes in CCND2 expression in classical monocytes between ATB baseline and 2–3 months after anti-tuberculosis treatment in 20 participants. Lines connect paired samples; dashed lines indicate the median expression levels in the

TB-negative and LTBI groups. The paired comparison was performed using the Wilcoxon signed-rank test.

*TB-negative, tuberculosis-negative control; LTBI, latent tuberculosis infection; ATB, active tuberculosis; AUC, area under the receiver operating characteristic curve; log_2CPM, log_2counts per million.

Supplementary Files

This is a list of supplementary files associated with this preprint. Click to download.

- SupplementaryTableS1.docx